9-1-2015

Fabrication of multianalyte CeO2 nanograin electrolyte–insulator–semiconductor biosensors by using CF4 plasma treatment

Chyuan Haur Kao
Chang Gung University

Hsiang Chen
National Chi Nan University

Fang Yao Stephen Hou
Marquette University, fangyaostephen.hou@marquette.edu

Shan Wei Chang
Chang Gung University

Che Wei Chang
Chang Gung University

See next page for additional authors

Published Version. *Sensing and Bio-Sensing Research,* Vol. 5 (September 2015): 71-77. DOI.

Authors
Chyuan Haur Kao, Hsiang Chen, Fang Yao Stephen Hou, Shan Wei Chang, Che Wei Chang, Chao Sung Lai, Chin Pang Chen, Yun Yang He, Shang-Ren Lin, Kun Min Hsieh, and Min Han Lin

Sensing and Bio-Sensing Research 5 (2015) 71–77

Contents lists available at ScienceDirect

Sensing and Bio-Sensing Research

journal homepage: www.elsevier.com/locate/sbsr

Fabrication of multianalyte CeO_2 nanograin electrolyte–insulator–semiconductor biosensors by using CF_4 plasma treatment

Chyuan Haur Kao [a,d], Hsiang Chen [b,*], Fang Yao Stephen Hou [c], Shan Wei Chang [a,d], Che Wei Chang [a,d], Chao Sung Lai [a,d], Chin Pang Chen [b], Yun Yang He [b], Shang-Ren Lin [b], Kun Min Hsieh [b], Min Han Lin [b]

[a] Department of Electronic Engineering, Chang Gung University, Taiwan, ROC
[b] Department of Applied Materials and Optoelectronic Engineering, National Chi Nan University, Taiwan, ROC
[c] Clinical Laboratory, Marquette University, USA
[d] Center for Biomedical Engineering, Chang Gung University, Taiwan, ROC

ARTICLE INFO

Article history:
Received 16 April 2015
Revised 27 June 2015
Accepted 1 July 2015

Keywords:
Multianalyte biosensor
CeO_2 nanograin
EIS
CF_4 plasma treatment
Membrane surface

ABSTRACT

Multianalyte CeO_2 biosensors have been demonstrated to detect pH, glucose, and urine concentrations. To enhance the multianalyte sensing capability of these biosensors, CF_4 plasma treatment was applied to create nanograin structures on the CeO_2 membrane surface and thereby increase the contact surface area. Multiple material analyses indicated that crystallization or grainization caused by the incorporation of flourine atoms during plasma treatment might be related to the formation of the nanograins. Because of the changes in surface morphology and crystalline structures, the multianalyte sensing performance was considerably enhanced. Multianalyte CeO_2 nanograin electrolyte–insulator–semiconductor biosensors exhibit potential for use in future biomedical sensing device applications.

1. Introduction

Over the past 10 years nanostructure-based biosensors have been intensively studied because of their distinct sensing capability [1,2]. It is commonly acknowledged that the biosensing properties of these sensors are not only relevant to their dimensions but also to their shapes [3–5]. Therefore, managing the morphologies of sensing membranes is a crucial and an efficient approach to acquiring preferable features [6,7]. Shape-controlled fabrication processes have been demonstrated, and nanostructures with various shapes such as cubes, wires, and rods have been designed using various synthesis techniques [8–10]. Because the surface contact area of a membrane can be enlarged and the number of the surface sites can be increased, biosensors with desirable morphologies can achieve high sensitivity and linearity [11,12]. Recently, EIS structures have been intensively investigated because of their simple structure and fast detection [13,14]. To enhance multianalyte sensing performance, various materials, alternative processes, and treatments such as annealing have been incorporated [15,16]. However, multianalyte biosensing EIS membranes with nanostructures on the membrane have not yet been clearly reported. In this research, we introduced CF_4 plasma treatment to shape nanostructures and, thus, increase the surface area and the number of surface sites of the membrane [17]. Nanograin structures formed using plasma treatment were observed in atomic force microscope (AFM) and scanning electron microscope (SEM) images [18]. Secondary ion mass spectroscopy (SIMS) results indicated that fluorine atoms on the membrane surface might be related to the formation of nanostructures. Consistent with the AFM and SEM images, X-ray diffraction (XRD) patterns and X-ray photoelectron spectroscopy (XPS) measurements confirmed that crystallization and grainization of CeO_2 might cause the formation of nanostructures [19]. The CeO_2 multianalyte biosensor demonstrated multiple sensing capability with solutions containing H^+, Na^+, K^+, glucose [20], and urea [21]. Furthermore, the results indicated that the formation of nanograins on the CeO_2 membrane further enhanced the multianalyte sensing capability of various electrolytes.

The impact of the development of nanograins on the understanding of the detecting film can be illustrated by considering the site-binding design in an explanation of the ionic consumption procedures at the electrolyte/oxide interface [13]. For pH detecting ability, the reaction voltage relies on the outer lining area prospective (ψ), which is an operation of the membrane content and the pH of the electrolyte [13,22]. The value of (ψ) can be calculated using Eq. (2).

* Corresponding author.
E-mail addresses: hchen@ncnu.edu.tw, chennew.boy@gmail.com (H. Chen).

http://dx.doi.org/10.1016/j.sbsr.2015.07.001
2214-1804/

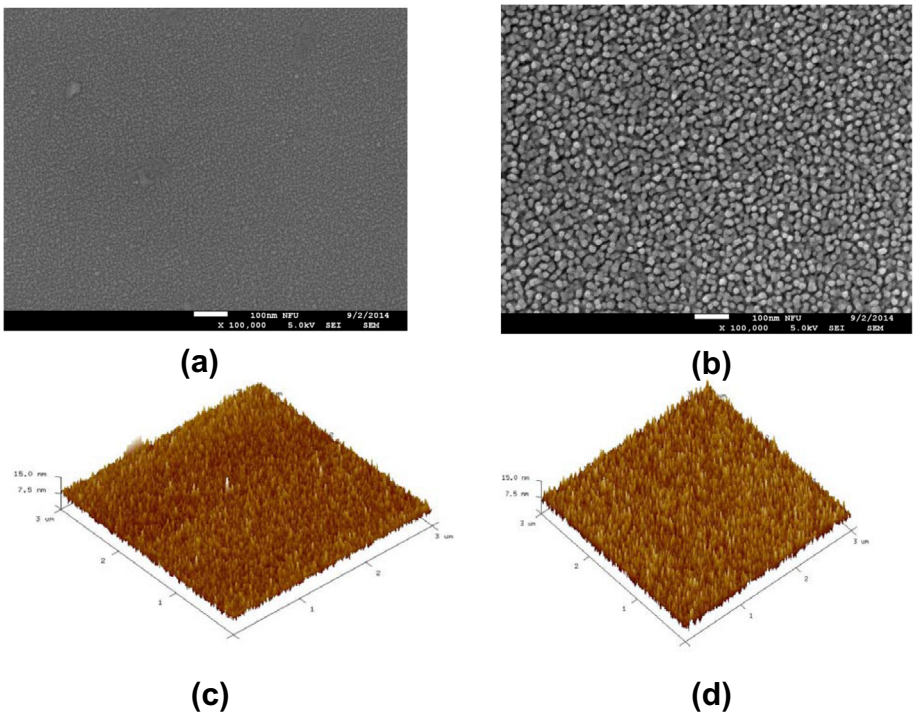

Fig. 1. FESEM images of the CeO_2 film (a) before and (b) after CF_4 plasma treatment for 15 s. AFM images of the CeO_2 film (c) before and (d) after CF_4 plasma treatment for 15 s.

The influence of the formation of nanograins on the detection of the sensing film can be understood by considering the site-binding model. To illustrate the ionic absorption procedures at the electrolyte/oxide interface involved in pH sensing, the detecting voltage on the surface potential (ψ) can be expressed as a function of the membrane material and the pH value of the electrolyte. The value of (ψ) can be calculated using Eq. (1).

$$\psi = 2.303\frac{kT}{q}\frac{\beta}{\beta+1}(\mathrm{pH}_{\mathrm{pzc}} - \mathrm{pH}) \quad (1)$$

where k is Boltzmann's constant, T is the temperature, q is the elementary charge, $\mathrm{pH}_{\mathrm{pzc}}$ is the pH value with zero charge, and β is a factor that signifies the chemical sensitivity of the gate oxide. Furthermore, the β value is proportional to the chemical sensitivity of the gate dielectric and is determined according to the density of surface hydroxyl groups, as described in Eq. (2).

$$\beta = \frac{2q^2\mathrm{Ns}\sqrt{K_aK_b}}{KTC_{\mathrm{DL}}} \quad (2)$$

where Ns is the count of surface site per unit area and C_{DL} is the double layer capacitance based on the Gouy–Chapman–Stern model [23]. According to Eqs. (1) and (2), a can be expected to result in a higher sensitivity and linearity in accordance with the value revealed in the report [24]. Nanograins formed through plasma treatment can noticeably increase the surface area and, hence, the surface sites; therefore, the sensing performance can be enhanced by incorporating plasma treatment.

2. Experimental details

EIS biosensors containing CeO_2 membranes were designed on 4-inch n-type (100) Si wafers with a resistivity of 5–10 Ω-cm. After RCA cleaning procedure, the wafers were dropped into 1% hydrofluoric acid to eliminate oxide from the surface. First, a 50-nm CeO_2 membrane was placed on the Si substrate through

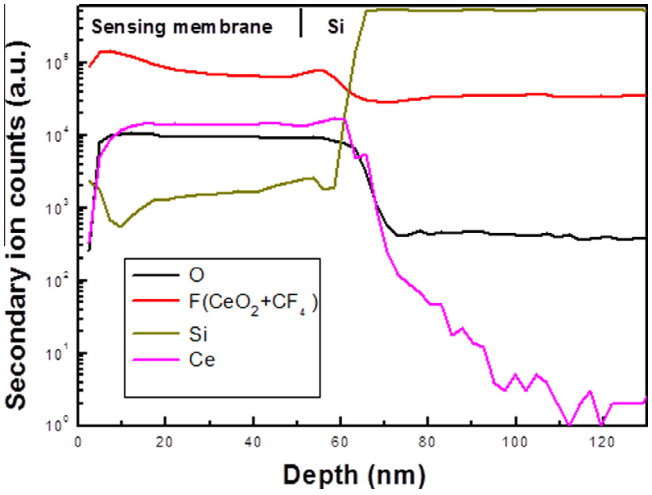

Fig. 2. SIMS profiles for the CeO_2 film treated with CF_4 plasma for 15 s.

radio frequency (rf) sputtering from a cerium target in a diluted O_2 ambient (Ar/O_2 = 20 sccm/5 sccm). The rf power and ambient pressure were 100 W and 20 mTorr, respectively. After deposition, CeO_2 membrane layers were subjected to a post-CF_4 treatment in a plasma-enhanced chemical vapor deposition system with an rf power of 30 W and a processing pressure of 500 mTorr for 15, 30, and 60 s, respectively. Subsequently, the back-side contact of the Si wafer was grown using a 300-nm Al film. The size of the sensing membrane was defined through photolithographic processing under a photosensitive epoxy (SU8-2005, Micro-Chem). EIS structures were then placed on the copper lines of a printed circuit board by using a silver gel. An epoxy package was included to separate the EIS structure and the copper line. The device structure is shown in the supplement data.

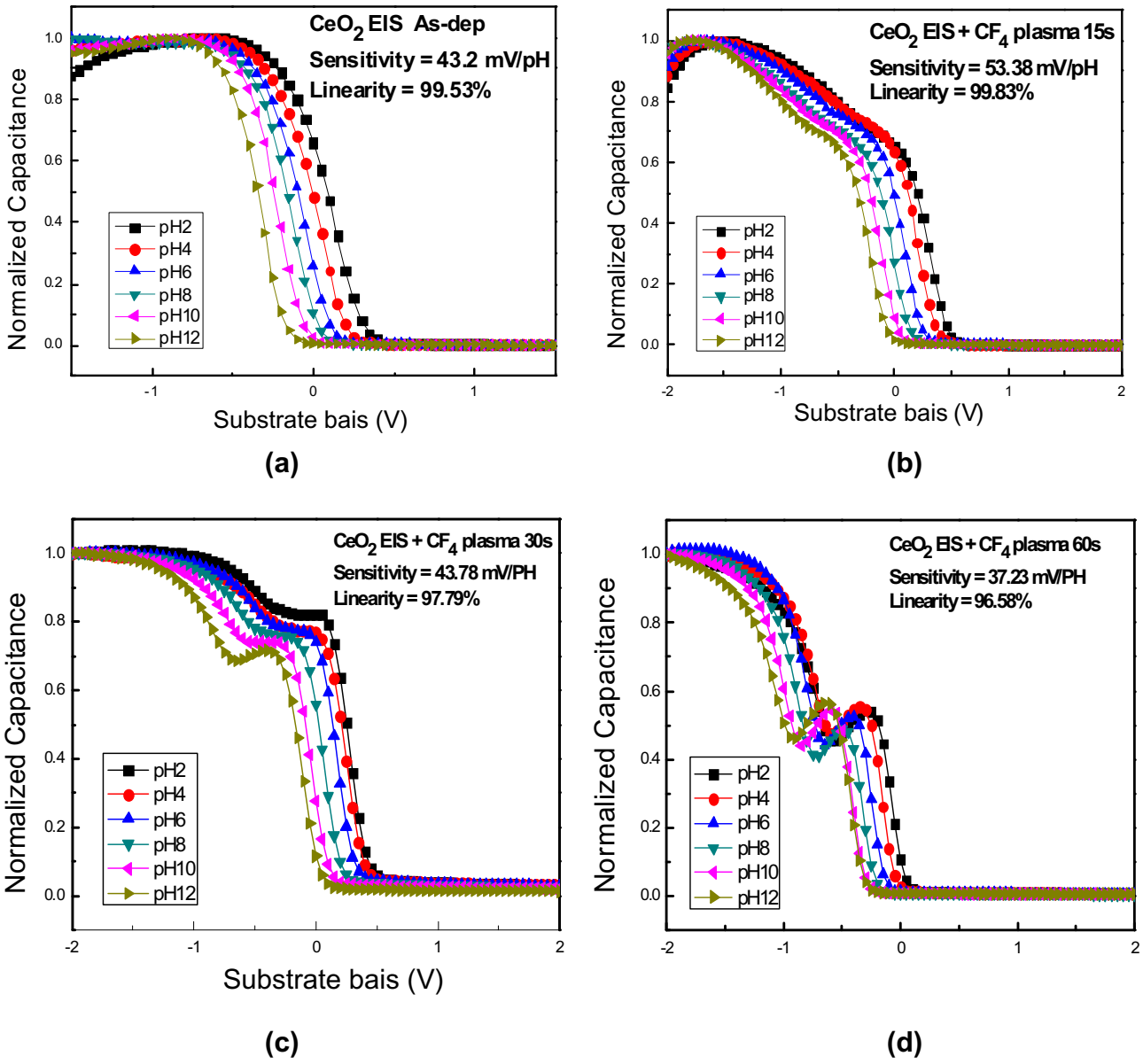

Fig. 3. C–V curves of (a) the as-deposited CeO_2 membrane and the CeO_2 membrane treated with CF_4 plasma for (b) 15 s, (c) 30 s, and (d) 60 s.

To examine the material properties of the sensing membrane, the CeO_2 membrane layer was analyzed using FESEM and AFM to investigate the nanograins. In addition, XRD and XPS were used to examine the crystalline structure and chemical bonds of the membrane layer. After the biosensor was fabricated and packed, the capacitance–voltage (C–V) curve was measured. To evaluate the sensing performance from the C–V curve, the responsive voltages for all devices were calculated using 0.4 C_{max} (C_{max}: maximum capacitance value in the C–V curve). We used 0.4 C_{max} as a standard line in the C–V curve and calculated the substrate-bias voltage changes after the device was submerged in solutions with various pH values. FESEM images were measured using a SM-7500F JEOL cold-field emission SEM. AFM images were taken using a Veeco D5000 AFM in tapping mode employing an applied nanosilicon tip with a 50-N/m spring constant. XRD was performed using XRD Bede D1. The X-ray source was Cu Kα (λ = 1.542 Å), and the XRD configuration was the Bragg–Brentano theta-2 theta. The diffraction angle 2θ ranged from 20° to 80° with a grazing incidence angle θ of 0.5°. The XPS spectra were performed using a VG ESCA Scientific Theta Probe (2002). The X-ray spot size, the take-off angle, and the pass energy were 15 μm, 53°, and 50 eV, respectively. The X-ray source for XPS was Al Kα (1486.6 eV). The C–V curves were measured using a precision LCR meter (HP-4284, Hewlett-112 Packard, USA).

3. Results and discussion

3.1. Material characterizations

To examine nanograins on the membrane surface, FESEM was used to reveal the surface morphology of the CeO_2 membrane layer before deposition of the metal contact. Before the CF_4 plasma treatment, the membrane surface was flat and no protruded nanostructures were observed, as shown in Fig. 1(a). After the film was treated with CF_4 plasma for 15 s, the nanograins on the surface formed, as shown in Fig. 1(b). The average size of a nanograin was 15 nm, and most of the grains exhibited a similar size, indicating that the CF_4 plasma could form uniform nanograins on the membrane surface. Consistent with the FESEM images, AFM analysis

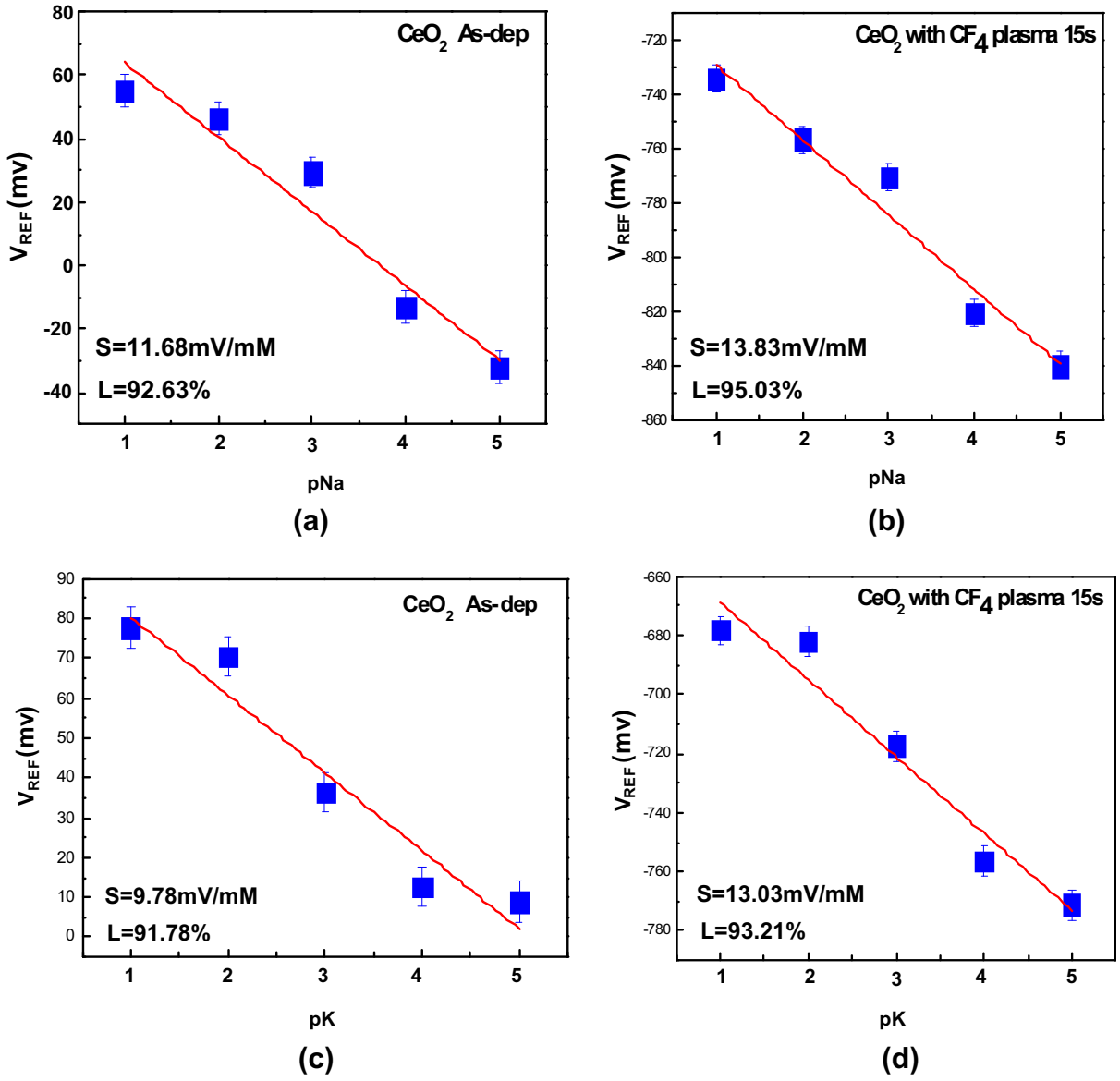

Fig. 4. pNa^+ sensing capability for the CeO_2 film (a) before and (b) after CF_4 plasma treatment for 15 s. pK^+ sensing capability of the CeO_2 film (c) before and (d) after CF_4 plasma treatment for 15 s.

revealed that uniform nanograins were generated on the membrane surface. After CF_4 plasma treatment, the membrane surface became rougher and nanograins were observed on the membrane surface, as shown in the AFM images in Fig. 1(c) and (d). The formation of the nanograin structures increased the surface area of the CeO_2 membrane. The number of surface sites, which is related to sensing capability, also increased.

To gain insight into the influence of CF_4 plasma treatment, SIMS measurement was performed. SIMS results, as shown in Fig. 2, revealed that fluorine atoms accumulated on the surface and piled up near the CeO_2/Si interface. The accumulation of fluorine atoms near the surface might result in the formation of Ce–F bonds and crystallization of the CeO_2 film near the surface as shown in the XRD and XPS analysis in the supplement information. Therefore, the incorporated fluorine atoms might have caused the formation of the CeO_2 nanograins owing to enhancement of binding. Furthermore, the fluorine atoms piled up near the CeO_2/Si might repair the dangling bonds, traps, and the defects near the interface and, thus, enhance the sensing performance of the CeO_2 membrane.

To investigate the sensing performance of the CeO_2 nanograin EIS biosensor, the pH sensitivity, pH linearity, hysteresis voltage, and drift rate were evaluated.

3.2. pH sensitivity and linearity

Fig. 3(a–d) show the C–V curves of the CeO_2 membrane and the sensing membrane treated with CF_4 plasma for 15, 30, and 60 s in a buffer solution with various pH values. The threshold voltage shift of the CeO_2 membranes revealed the sensitivity of the device and was as high as 55.88 mV/pH. The sensitivities of the as-deposited membrane and the CeO_2 membranes that underwent plasma treatment for 15, 30, and 60 s were 43.20, 53.38, 43.78, and 37.23 mV/pH, respectively, as shown in the supplement data. As observed in the material analysis, the CeO_2 treated in plasma for 15 s exhibited the highest sensitivity. Furthermore, the pH sensing membrane that underwent CF_4 plasma treatment for 15 s exhibited excellent linearity of 99.83. This was attributed to the formation of nanograins on the surface CeO_2 membrane after plasma processing. The formation of the nanograins enlarged the

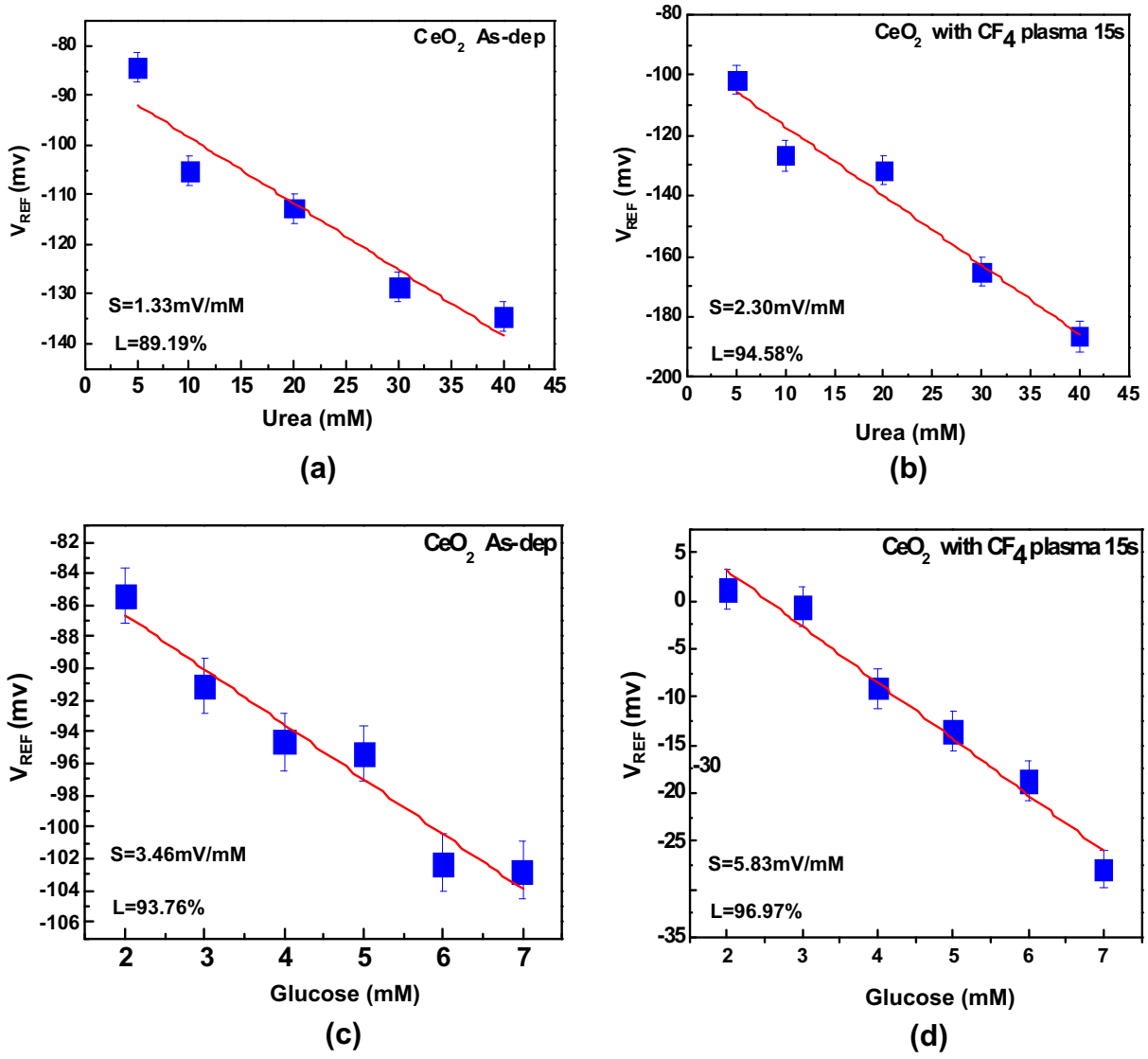

Fig. 5. Urea sensing properties of (a) the as-deposited CeO_2 membrane and (b) the membrane treated with CF_4 plasma for 15 s. Glucose sensing properties of (c) the as-deposited CeO_2 membrane and (d) the membrane treated with CF_4 plasma for 15 s.

membrane surface contact area and increased the surface sites. Therefore, the sensitivity and linearity were noticeably enhanced. However, as the plasma treatment time increased to 30 and 60 s, the sensing performance deteriorated; the material analysis revealed that the long plasma treatment damaged the surface. The hysteresis voltage, and drift rate are presented in the supplement data.

3.3. Multianalyte sensing properties

In addition to pH sensing, the concentration of biologically relevant ions is a crucial indicator associated with patient heath conditions. Therefore, various methods for detecting potassium ion (K^+) and sodium ion (Na^+) concentrations have been employed in biomedical research [25]. In addition, K^+ and Na^+ ion concentrations are crucial indicators of food and wine quality and water pollution [26].

The K^+ ion and Na^+ ion sensing properties of the CeO_2 membranes were analyzed. We measured the sensitivity of the as-deposited CeO_2 sensing membrane and the membrane treated with CF_4 plasma for 15 s. First, a 5 mM Tris/HCl buffer solution, of which the pH value was kept at 8.7, was prepared [27]. A micropipette was used to control the concentrations of Na^+ and K^+ ions in the range between 10^{-5} to 10^{-1} M while 1 M NaCl/Tris–HCl and 1 M KCl/Tris–HCl were injected into the buffer electrolyte. Subsequently, the pNa sensitivity of the as-deposited CeO_2 membrane and the CeO_2 membrane treated with plasma for 15 s was calculated, as shown in Fig. 4(a) and (b). Moreover, the pK sensitivity of the as-deposited CeO_2 membrane and the CeO_2 membrane treated with plasma for 15 s was calculated, as shown in Fig. 4(c) and (d). The pNa and pK sensitivity values of the as-deposited CeO_2 sensing membrane were 11.68 mV/pNa and 9.78 mV/pK, respectively. After the membrane was treated with CF_4 plasma for 15 s, the pNa and pK sensitivity of the sensing membrane were increased to 13.83 mV/pNa and 13.03 mV/pK, respectively. The EIS structure containing nanograins was more sensitive to Na^+ and K^+ than that without nanostructures.

A CeO_2 nanograin sensing membrane on an EIS structure was used to detect urine concentrations in solutions. Monitoring urea concentrations by using biosensors is of great interest in biomedical applications. The concentration of urea in blood is a crucial indicator of patient constitution and used in disease evaluation.

Because enzymatic reactions usually produce ionic species, selective detection of various chemicals involves using ion-selective membranes with appropriate enzymes. To stabilize biosensor properties and lengthen their lifetimes, various methods of enzyme immobilization, such as physical adsorption [28], entrapment [30], covalent bonding [29], and cross-linking have been proposed. In this study, we established a process for immobilizing urease by using covalent bonding methods [31]. The developed CeO_2 nanograin EIS biosensor facilitated investigating the pUrea sensing performance.

The following is the equation of the urea hydrolysis reaction catalyzed by urease:

$$NH_2CONH_2 + 3H_2O \rightarrow 2NH_4^+ + OH^- + HCO_3^-$$

The generated hydrogen ions and ammonium ions can be used for urea detection. The variation of the pH value caused by an enzyme-catalyzed reaction can lead to changes in the analytical output signal of a sensor.

To study the urea sensing properties of the CeO_2 nanograin sensing membrane, the urea sensitivity and linearity were measured in solutions in which the urea concentration was controlled in a range between 5 and 40 mM. As shown in Fig. 5(a) and (b), the as-deposited CeO_2 membranes exhibited a urea sensitivity of 1.33 mV/mM and linearity of 89.19%; the CeO_2 membranes with nanostructures after CF_4 plasma treatment exhibited a higher sensitivity of 2.30 mV/mM and a higher linearity of 94.58%. The results indicated that incorporating nanostructures onto the membrane surface enhanced the urea sensing performance as well as the capability to sense H^+, Na^+, and K^+.

We used an enzymatic EIS-based membrane similar to that used in urea detection for glucose detection. Glucose oxidase was used as the biocomponent, and the biosensor measured the glucose concentration by measuring the changes in pH values caused by the generation of hydrogen ions with the dissociation of glucose acid. The chemical formula for the hydrolysis of glucose by glucose oxidase is as follows:

$$\beta\text{-D-Glucose} + O_2 + H_2O \xrightarrow{\text{glucose oxidase}} \text{D-glucose-}\delta\text{-lactone} + H_2O_2$$

$$\text{D-Glucose-}\delta\text{-lactone} \rightarrow \text{D-gluconoate} + H^+$$

Similarly, the procedure of glucose immobilization was achieved by employing covalent bonding methods. To examine the glucose sensing properties, the CeO_2 sensing membrane on the EIS structure was used to measure the glucose concentrations in solutions in which the glucose concentration was controlled in a range between 2 and 7 mM. As shown in Fig. 5(c) and (d), the as-deposited CeO_2 membranes exhibited a low glucose sensitivity of 3.46 mV/mM and linearity of 93.76%. After the membrane was incorporated with nanostructures through plasma treatment, the sensitivity increased to 5.83 mV/mM and the linearity increased to 94.58%. The results revealed that nanostructures on the membrane enhanced the multianalyte sensing performance because of the increase of the contact area and the surface sites and suppression of defects. After the nanograins were incorporated through CF_4 plasma treatment, the capability to sense multiple analytes, namely H^+, Na^+, K^+, urea, and glucose, was improved.

4. Conclusion

In this study, multianalyte CeO_2 nanograin EIS biosensors were fabricated. Nanograin structures formed on top of the CeO_2 membrane surface, as shown in FESEM and AFM images. The formation of nanostructures through CF_4 plasma treatment for an appropriate time of 15 s was associated with enhanced crystalline structures and stronger chemical binding, as indicated by XRD and XPS measurements. Furthermore, adding fluorine atoms during the plasma treatment process might have been related to the formation of the nanostructures, as indicated by SIMS measurements. Therefore, incorporating nanostructures can enhance the performance of biosensors. A higher sensitivity, higher linearity, lower hysteresis voltage, and lower drift ratio of pH sensing was achieved. Moreover, the capability to sense multiple analytes, namely H^+, Na^+, K^+, urea, and glucose, was achieved by incorporating nanostructures onto the membrane surface, thereby increasing the membrane surface contact area and the effective surface sites. Multianalyte CeO_2 nanograin EIS biosensors exhibit potential for use in future biomedical sensing device applications.

Acknowledgments

This study was supported by the National Science Council (NSC) Taiwan, Republic of China, under Contract No. 102-2221-E-260-008.

Appendix A. Supplementary data

Supplementary data associated with this article can be found, in the online version, at http://dx.doi.org/10.1016/j.sbsr.2015.07.001.

References

[1] T.-E. Bae, H.-J. Jang, J.-H. Yang, W.-J. Cho, High performance of silicon nanowire-based biosensors using a high-k stacked sensing thin film, ACS Appl. Mater. Interfaces 5 (11) (2013) 5214–5218.
[2] L. Santos, J.P. Neto, A. Crespo, D. Nunes, N. Costa, I.M. Fonseca, P. Barquinha, L. Pereira, J. Silva, R. Martins, WO3 nanoparticle-based conformable pH sensor, ACS Appl. Mater. Interfaces 6 (15) (2014) 12226–12234.
[3] G. Das, F. Mecarini, F. Gentile, A.F. De, K.H. Mohan, P. Candeloro, C. Liberale, G. Cuda, F.E. Di, Nano-patterned SERS substrate: application for protein analysis vs. temperature, Biosens. Bioelectron. 24 (6) (2009) 1693–1699.
[4] R. Kim, N. Hong, Y. Nam, Gold nanograin microelectrodes for neuroelectronic interfaces, Biotechnol. J. 8 (2) (2013) 206–214.
[5] Y. Li, F. Huang, J. Chen, T. Mo, S. Li, F. Wang, S. Feng, Y. Li, A high performance enzyme-free glucose sensor based on the graphene-CuO nanocomposites, Int. J. Electrochem. Sci. 8 (2013) 6332–6342.
[6] F. Cao, J. Gong, Nonenzymatic glucose sensor based on CuO microfibers composed of CuO nanoparticles, Anal. Chim. Acta 723 (2012) 39–44.
[7] M. Masood, S. Chen, E. Carlen, A.v.d. Berg, All-(1 1 1) Surface silicon nanowires: Selective functionalization for biosensing applications, ACS Appl. Mater. Interfaces 2 (12) (2010) 3422–3428.
[8] M. Das, C. Dhand, G. Sumana, A.K. Srivastava, R. Nagarajan, L. Nain, M. Iwamoto, T. Manaka, B.D. Malhotra, Electrophoretic fabrication of chitosan-zirconium-oxide nanobiocomposite platform for nucleic acid detection, Biomacromolecules 12 (3) (2011) 540–547.
[9] L. Tian, X. Zhong, W. Hu, B. Liu, Y. Li, Fabrication of cubic PtCu nanocages and their enhanced electrocatalytic activity towards hydrogen peroxide, Nanoscale Res. Lett. 9 (1) (2014) 68. pp. 61–65.
[10] X. Wang, C. Hu, H. Liu, G. Du, X. He, Y. Xi, Synthesis of CuO nanostructures and their application for nonenzymatic glucose sensing, Sens. Actuators B 144 (1) (2010) 220–225.
[11] J.-L. Her, M.-H. Wu, Y.-B. Peng, T.-M. Pan, W.-H. Weng, S.-T. Pang, L. Chi, High performance $GdTi_xO_y$ electrolyte-insulator-semiconductor pH sensor and biosensor, Int. J. Electrochem. Sci. 8 (1) (2013) 606–620.
[12] C.-H. Kao, H. Chen, L.-T. Kuo, J.-C. Wang, Y.-T. Chen, Y.-C. Chu, C.-Y. Chen, C.-S. Lai, S.W. Chang, C.W. Chang, Multi-analyte biosensors on a CF_4 plasma treated Nb_2O_5-based membrane with an extended gate field effect transistor structure, Sens. Actuators B 194 (2014) 419–426.
[13] C.D. Fung, P.W. Cheung, W.H. Ko, A generalized theory of an electrolyte-insulator-semiconductor field-effect transistor, IEEE Trans. Electron Devices 33 (1) (1986) 8–18.
[14] Y. Nishikawa, T. Yamaguchi, M. Yoshiki, H. Satake, N. Fukushima, Interfacial properties of single-crystalline CeO_2 high-k gate dielectrics directly grown on Si (1 1 1), Appl. Phys. Lett. 81 (23) (2002) 4386–4388.
[15] R.-A. Doong, H.-M. Shih, Array-based titanium dioxide biosensors for ratiometric determination of glucose, glutamate and urea, Biosens. Bioelectron. 25 (6) (2010) 1439–1446.
[16] N.-Q. Jia, Z.-R. Zhang, J.-Z. Zhu, G.-X. Zhang, Multianalyte biosensor for simultaneous determination of glucose and galactose based on micromachined chamber-type electrodes, Chin. J. Chem. 22 (9) (2004) 908–912.
[17] S. Kunuku, K.J. Sankaran, C.-Y. Tsai, W.-H. Chang, N.-H. Tai, K.-C. Leou, I.N. Lin, Investigations on diamond nanostructuring of different morphologies by the

reactive-ion etching process and their potential applications, ACS Appl. Mater. Interfaces 5 (15) (2013) 7439–7449.
[18] M.-H. Wu, H.-W. Yang, M.-Y. Hua, Y.-B. Peng, T.-M. Pan, High-κ GdTixOy sensing membrane-based electrolyte-insulator-semiconductor with magnetic nanoparticles as enzyme carriers for protein contamination-free glucose biosensing, Biosens. Bioelectron. 47 (2013) 99–105.
[19] S.-W. Choi, J.Y. Park, S.S. Kim, Growth behavior and sensing properties of nanograins in CuO nanofibers, Chem. Eng. J. 172 (1) (2011) 550–556.
[20] B. Fang, A. Gu, G. Wang, W. Wang, Y. Feng, C. Zhang, X. Zhang, Silver oxide nanowalls grown on Cu substrate as an enzymeless glucose sensor, ACS Appl. Mater. Interfaces 1 (12) (2009) 2829–2834.
[21] H. Barhoumi, A. Maaref, M. Rammah, C. Martelet, N. Jaffrezic, C. Mousty, S. Vial, C. Forano, Urea biosensor based on Zn_3Al–Urease layered double hydroxides nanohybrid coated on insulated silicon structures, Mater. Sci. Eng. C 26 (2) (2006) 328–333.
[22] S. Jamasb, S.D. Collins, R.L. Smith, A physical model for threshold voltage instability in Si 3 N 4-gate H+-sensitive FET's (pH ISFET's), IEEE Trans. Electron Devices 45 (6) (1998) 1239–1245.
[23] R. Van Hal, J. Eijkel, P. Bergveld, A novel description of ISFET sensitivity with the buffer capacity and double-layer capacitance as key parameters, Sens. Actuators B 24 (1) (1995) 201–205.
[24] M.-N. Niu, X.-F. Ding, Q.-Y. Tong, Effect of two types of surface sites on the characteristics of Si_3N_4-gate pH-ISFETs, Sens. Actuators B 37 (1) (1996) 13–17.
[25] C.-M. Yang, T.-F. Lu, K.-I. Ho, J.-C. Wang, D.G. Pijanowska, B. Jaroszewicz, C.-S. Lai, HfOxFy based ISFETs with reactive fluorine doping for K ion detection, Int. J. Electrochem. Sci. 9 (2014) 7069–7082.
[26] J. Alonso, J. Artigas, C. Jimenez, Analysis and identification of several apple varieties using ISFETs sensors, Talanta 59 (6) (2003) 1245–1252.
[27] A. Errachid, J. Bausells, N. Zine, H. Jaffrezic, C. Martelet, N. Jaffrezic-Renault, M. Charbonnier, Analytical features of K+-sensitive membrane obtained by implantation in silicon dioxide films, Mater. Sci. Eng. C 21 (1) (2002) 9–13.
[28] C.J. Patton, S. Crouch, Spectrophotometric and kinetics investigation of the Berthelot reaction for the determination of ammonia, Anal. Chem. 49 (3) (1977) 464–469.
[29] F. Roch-Ramel, An enzymic and fluorophotometric method for estimating urea concentrations in nanoliter specimens, Anal. Biochem. 21 (3) (1967) 372–381.
[30] J. Růžička, E.H. Hansen, Flow injection analysis. Principles, applications and trends, Anal. Chim. Acta 114 (1980) 19–44.
[31] M. Şenel, C. Nergiz, Novel amperometric glucose biosensor based on covalent immobilization of glucose oxidase on poly (pyrrole propylic acid)/Au nanocomposite, Curr. Appl. Phys. 12 (4) (2012) 1118–1124.